PLOS ONE

RESEARCH ARTICLE

The involvement of CYP1A2 in biodegradation of dioxins in pigs

Sylwia Swigonska[1☯*], **Tomasz Molcan**[2☯], **Anna Nynca**[1], **Renata E. Ciereszko**[1,3]

1 Laboratory of Molecular Diagnostics, Faculty of Biology and Biotechnology, University of Warmia and Mazury in Olsztyn, Olsztyn, Poland, **2** Department of Bioinformatics, Institute of Biochemistry and Biophysics, Polish Academy of Sciences, Warsaw, Poland, **3** Department of Animal Anatomy and Physiology, Faculty of Biology and Biotechnology, University of Warmia and Mazury in Olsztyn, Olsztyn, Poland

☯ These authors contributed equally to this work.
* sylwia.swigonska@uwm.edu.pl

Citation: Swigonska S, Molcan T, Nynca A, Ciereszko RE (2022) The involvement of CYP1A2 in biodegradation of dioxins in pigs. PLoS ONE 17(5): e0267162. https://doi.org/10.1371/journal.pone.0267162

Editor: Emilio Gallicchio, Brooklyn College of the City University of New York, UNITED STATES

Received: November 4, 2021

Accepted: March 29, 2022

Published: May 26, 2022

Data Availability Statement: All relevant data are within the paper, its Supporting Information files, and in GenBank under the following accession number: AIY35109.1.

Funding: This study was supported by National Science Centre, Poland (2016/21/N/NZ9/02320, 2012/05/B/NZ9/03333) and The Ministry of Science and Higher Education in Poland (UWM No. 528.0206.0806). This research was supported in part by PLGrid Infrastructure. There was no additional external funding received for this study. The funders had no role in study design, data

Abstract

2,3,7,8-tetrachlorodibenzo-*p*-dioxin (TCDD) is one of the most harmful chemicals showing resistance to biodegradation. The majority of TCDD effects is mediated by the aryl hydrocarbon receptor (AhR) pathway. TCDD binding to AhR results in the activation of cytochrome P450 enzymes (CYP1A1, CYP1A2, CYP1B1) involved in dioxin biodegradation. The goal of the study was to explore the potential role of CYP1A2 in the metabolism of TCDD. We investigated a molecular structure of CYP1A2 and the binding selectivity and affinity between the pig CYP1A2 and: 1/ DiCDD or TCDD (dioxins differing in toxicity and biodegradability) or 2/ their selected metabolites. pCYP1A2 demonstrated higher affinity towards DiCDD and TCDD than other pCYP1 enzymes. All dioxin-pCYP1A2 complexes were found to be stabilized by hydrophobic interactions. The calculated distances between the heme oxygen and the dioxin carbon nearest to the oxygen, reflecting the hydroxylating potential of CYP1A2, were higher than in other pCYP1 enzymes. The distances between the heme iron and the nearest dioxin carbon exceeded 5 Å, a distance sufficient to allow the metabolites to leave the active site. However, the molecular dynamics simulations revealed that two access channels of CYP1A2 were closed upon binding the majority of the examined dioxins. Moreover, the binding of dioxin metabolites did not promote opening of channel S–an exit for hydroxylated products. It appears that the undesired changes in the behavior of access channels prevail over the hydroxylating potential of CYP1A2 towards TCDD and the favorable distances, ultimately trapping the metabolites at the enzyme's active site.

1. Introduction

The global awareness concerning environmental pollutants is constantly growing. This is due to decades of industrialization which offered not only needed or desirable goods but also flooded us with waste by-products. Such by-products include polychlorinated dibenzo-*p*-dioxins (PCDDs, dioxins) that persistently contaminate our environment. The largest unintentional release of 2,3,7,8-tetrachlorodibenzo-*p*-dioxin (TCDD),the most toxic amongst 75 known dioxin congeners, occurs through waste incineration, metal production as well as

collection and analysis, decision to publish, or preparation of the manuscript.

Competing interests: The authors have declared that no competing interests exist.

petrol industry and wood combustion [1]. TCDD is considered to be one of the most harmful chemicals with long-lasting half-life (e.g., 8–10 years in humans). Exposure to TCDD results in numerous pathophysiological abnormalities such as chloracne, thymic atrophy and immune dysfunction, hepatic damage and steatosis, gastric epithelial hyperplasia, embryonic teratogenesis and cancer [2]. TCDD also affects male and female reproduction as well as endocrinology. It alters sexual behavior, decreases spermatogenesis, diminishes fertility, causes endometriosis, teratogenesis and abortion [3]. Moreover, the dioxin influences thyroid hormone metabolism as well as steroid hormone secretion [4, 5]. In pigs, TCDD was also found to affect the expression of genes involved in the regulation of granulosa cell cycle, proliferation and follicular atresia [6, 7].

Toxicity of dioxins is conditioned by the number and position of chlorine atoms present in its molecule. Dioxin congeners substituted in lateral positions with chlorine atoms, usually demonstrate high level of toxicity [8–10]. The extremely high toxicity of TCDD results from the occurence of chlorine atoms in all lateral positions and is accompanied by the highest resistance to biodegradation [9, 10] (. In contrast, 2,7-dichlorodibenzo-*p*-dioxin (DiCDD), less toxic than TCDD and containing unsubstituted lateral positions, appears to be effectively metabolized [11, 12]. TCDD's high resistance to biodegradation results in its accumulation in adipose tissue and hence is, at least partially, responsible for its adverse effects exerted on living organisms [10, 13, 14]. It should be noted that both, toxicity and susceptibility of PCDDs to biodegradation are not only determined by a dioxin chemical structure but also are species-dependent [9, 10].

The majority of PCDD effects is mediated by the aryl hydrocarbon receptor (AhR) pathway. AhR is a highly conserved transcription factor activated by numerous exogenous ligands, including PCDDs, polyhalogenated dibenzofurans (PCDFs) and polyaromatic hydrocarbons (PAHs) [15]. The TCDD binding to AhR results in the translocation of the TCDD-AhR complex to the nucleus and dimerization with AhR nuclear translocator (ARNT). The TCDD-AhR-ARNT complex binds a dioxin response element (DRE) in promoter regions of TCDD target genes including those of phase I biotransformation enzymes, e.g., cytochrome P450 (CYP1) family 1. CYP1A1, CYP1A2 and CYP1B1 are involved in the biodegradation of PCDDs and PAHs. In addition to contribution to phase 1 metabolism of drugs and xenobiotics, the enzymes play also a role in the development of many diseases including cancer [16].

The detoxification process starts with reactions of hydroxylation occurring in heme-containing active site of the enzyme [8, 15, 17, 18]. In our previous studies we analyzed the potential of pig CYP1A1 (pCYP1A; [12]) and CYP1B1 [19] to hydroxylate dioxins differing in toxicity and biodegradability. We have reported that TCDD, but not DiCDD, was not effectively metabolized by pCYP1A1 in pigs mainly due to the specific behavior of substrate channels leading into the active site of the enzyme. *In silico* analysis demonstrated that TCDD, upon its binding by CYP1A1, is not able to leave the enzyme's active site because of the closure of the access channels [12]. Similar analysis performed for pig CYP1B1 demonstrated a smaller distance between heme oxygen and the nearest TCDD carbon atom, reflecting the higher hydroxylating potential of pig CYP1B1 than CYP1A1 [19]. Additionally, compared to CYP1A1, TCDD binding to the CYP1B1 active site results in a higher availability of access channel S–considered to be an exit channel for hydroxylation products [19, 20]. On the other hand, the smaller volume of the CYP1B1 active site may hinder the mobility of TCDD molecule. This fact together with the long half-life of TCDD associated with ineffective biodegradation suggests that there are other factors inhibiting hydroxylation of the dioxin. However, the exact mechanism responsible for this inhibition within both CYPs is still not recognized. Therefore, CYP1A2, the last member of the CYP1 family, directly involved in the metabolism of xenobiotics [21] was a natural candidate for testing its ability to metabolize dioxins.

Different dynamics of the loop-like structures forming the substrate binding cavity of a particular CYP1 enzyme additionally justify the idea to explore the dioxin-CYP1A2 complexes. Moreover, contrary to CYP1A1 and CYP1B1, ubiquitously distributed in many animal tissues, the presence of CYP1A2 is limited mainly to the liver [22, 23] which may also affect functioning of the enzyme.

It is commonly known that, contrary to other dioxins, biodegradation of TCDD is extremely slow and inefficient. However, a few *in vitro* and *in vivo* studies demonstrated the generation of several mono-hydroxylated TCDD metabolites in humans, rats and dogs [9, 11, 14, 24, 25]. Therefore, in addition to TCDD and DiCDD, some selected primary TCDD metabolites as well as their molecular interactions with CYP1A2 were examined in the current study. The main goal of the present study was to explore the potential role of CYP1A2 in the metabolism of PCDDs in the pig. To achieve this goal, we investigated *in silico* a molecular structure of CYP1A2 as well as the binding selectivity and affinity between the pig CYP1A2 and DiCDD or TCDD, the two dioxins differing in toxicity and biodegradability. Similar analysis was also performed for four selected dioxin metabolites. In addition, the accessibility of CYP1A2 access channels upon binding of dioxins and their metabolites was investigated.

2. Results

2.1. In silico model of the pig CYP1A2 catalytic domain

The similarity level of the CYP1A2 amino acid (aa) sequence between the pig and other species ranged from71.40% (*Mus pahari*) to 86.05% (*Camelus ferus*) (S1 Table, Fig 1). It was also found that aa sequence of pCYP1A2 shared 81.40% homology with human CYP1A2 (S1 Fig). The tertiary structure of the pCYP1A2 catalytic domain is shown in Fig 2A. The pCYP1A2 protein is composed of 12 canonical α-helices (A-L) and six β-sheets (β1- β6). In addition, the spatial structure of pCYP1A2 includes three short helices (B′, F′ and K′) anchored in the membrane. These helices are frequently involved in the formation of substrate channels within the enzyme active site. A characteristic three-aa break (221–223) in helix F, typical for mammalian pCYP1A2 enzymes, was also found in the pig (S1 Fig). The PROCHECK evaluation of the final pCYP1A2 model revealed that 94.2% of its residues were located in the most favorable region (red) of Ramachandran plot (S2 Fig). The Z-score provided by ProSA-web indicated the overall pCYP1A2 model quality as -9.34, while the overall model quality for human CYP1A2 was estimated at-10.28.Moreover, the model evaluation performed by VERIFY3D indicated that 94.0%of residues produced scores higher than 0.2. The achieved results confirm that the generated homology-based model of pCYP1A2 protein is characterized by high quality parameters and therefore highly reliable.

We have also shown that the deeply buried active site of the pCYP1A2 was bordered by K-β1 and B-C loops, G, I, B′ and F helix regions and β4 sheet (Fig 2). The volume of the active site was calculated to be 436.98 $Å^3$.

The pig CYP1A2 protein was used as reference. Letter codes in the first (outer) circle indicate the alignment position and the amino acid code of the reference sequence. The colored square boxes of the second circle indicate the MSA position conservation (highly conserved positions are presented in red, while less conserved in blue). The third circle shows the cumulative mutual information as histograms, facing outwards. In the center of the circle lines can be observed, that connect pairs of positions with mutual information greater than 6.5. Red edges represent the top 5%, black lines represent points scoring between 95–70%, and gray edges account for the remaining 70%.

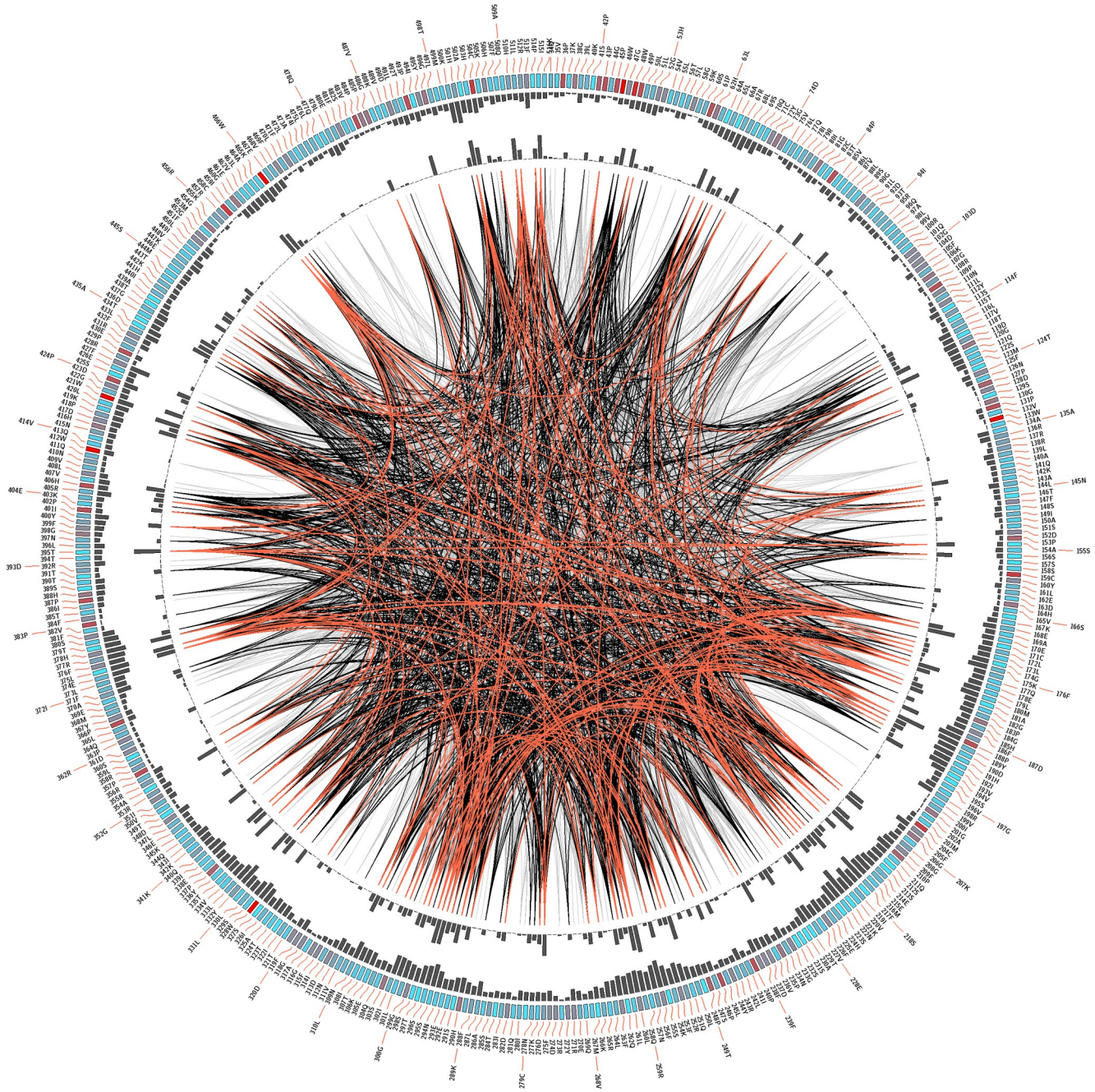

Fig 1. CIRCOS analysis of CYP1A2 i.e., interspecies alignment of the enzyme sequence.

https://doi.org/10.1371/journal.pone.0267162.g001

2.2. Docking and molecular dynamics simulation of the PCDD-porcine CYP1A2 complexes

Molecular docking confirmed the high reliability of the constructed pCYP1A2 model. All examined dioxins (DiCDD, TCDD and four metabolites) assumed the same orientation within the CYP1A2 active site (S3 Fig). The amino acids involved in the stabilization of a particular dioxin molecule within the enzyme active site are presented in Table 1. The dioxins were

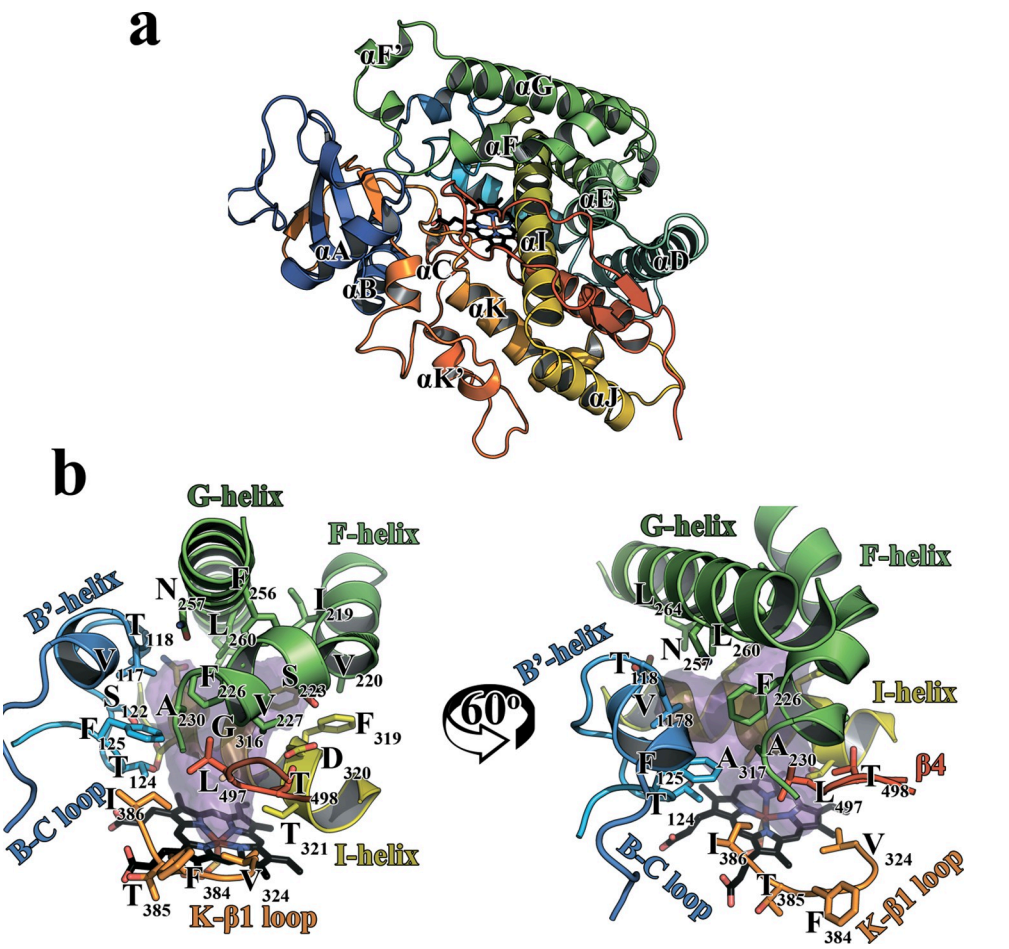

Fig 2. The overall three-dimensional structure of pig CYP1A2 (pCYP1A2) catalytic domain **(a).** The N-terminal end of the amino acid chain is marked in dark blue, the C-terminal end is marked in red; different letters and colors (A–L) depict 12 α-helices of the protein. Topology of the pCYP1A2 active site (b). The active site of pCYP1A2 is presented as a violet area. Heme molecule of the active site is shown in black. Residues bordering the active site are depicted as color sticks. Helices (G, I, B′, F) and loops (B-C, K-β1) surrounding the active site are shown in different colors. A characteristic three-aa break (221–223) in helix F, typical for mammalian pCYP1A2 enzymes, is visible in the aa sequence.

https://doi.org/10.1371/journal.pone.0267162.g002

found to be stabilized by hydrophobic interactions including π-stacking interactions between a dioxin molecule and the residues of the pCYP1A2.

During MD simulation the complexes reached equilibrium after the first 100 ns of the simulation (Fig 3, S2 Table). To examine the potential of the pCYP1A2 to hydroxylate dioxin congeners, the distance between the heme oxygen atom and the dioxin carbon atom nearest to the oxygen was calculated. The calculated distances oscillated around 3.36 ± 0.42Å for DiCDD and 3.50 ± 0.22 Å for TCDD (Fig 4A and 4B). In addition, the angle between the heme iron, oxygen and the dioxin carbon atom that is nearest to the oxygen was also measured. This angle oscillated around 138.42 ± 0.06˚ and 144.92 ± 0.04˚ for DiCDD and TCDD, respectively (Fig 4C and 4D). The visualization of a particular dioxin position within the active site of pCYP1A2 during MD simulation is presented in Fig 5. All examined congeners were located in the pCYP1A2 active site directly above the heme. Dioxin molecules were found to be stabilized in the active site solely by hydrophobic interactions (Table 1, Fig 5). Each dioxin was stabilized

Table 1. The pCYP1A2 residues involved in molecular interactions with the examined dioxins.

Compounds	After molecular docking		AfterMD simulations	
	Hydrophobic interactions	π-π interactions	Hydrophobic interactions	π-π interactions
DiCDD	**L_{260}** **G_{316}** **A_{317}** T_{321} V_{382} **I_{386}**	F_{125} **F_{226}**	T_{124} **G_{316}** **A_{317}** **T_{321}** V_{382} I_{386} **L_{497}**	F_{125} **F_{226}**
3OH-DiCDD	T_{124} S_{223} V_{227} **L_{260}** **G_{316}** **A_{317}** D_{320} T_{321} **I_{386}**	**F_{226}** F_{256}	N_{257} L_{260} N_{312} **G_{316}** **A_{317}** **T_{321}** **L_{497}**	F_{125} **F_{226}**
TCDD	T_{124} S_{223} **L_{260}** **G_{316}** **A_{317}** D_{320} **I_{386}**	**F_{226}** F_{256}	**G_{316}** **A_{317}** D_{320} **T_{321}** V_{382} I_{386} **L_{497}**	F_{125} **F_{226}** F_{319}
8OH-TriCDD	**L_{260}** **G_{316}** **A_{317}** T_{321} V_{382} **I_{386}** T_{498}	F_{125} **F_{226}** F_{256}	L_{260} **G_{316}** **A_{317}** **T_{321}** V_{382} I_{386} **L_{497}**	F_{125} **F_{226}** F_{319}
1OH-TCDD	T_{124} S_{223} V_{227} **L_{260}** **G_{316}** **A_{317}** D_{320} T_{321} V_{382} **I_{386}** T_{498}	**F_{226}** F_{256}	T_{118} T_{124} L_{260} **G_{316}** **A_{317}** **T_{321}** V_{382} I_{386} **L_{497}**	F_{125} **F_{226}** F_{319}
2OH-TCDD	T_{124} **L_{260}** N_{312} **G_{316}** **A_{317}** T_{321} V_{382} **I_{386}** T_{498}	F_{125} **F_{226}** F_{256}	T_{124} S_{223} G_{227} L_{260} **G_{316}** **A_{317}** **T_{321}** V_{382} I_{386} **L_{497}** T_{498}	**F_{226}** F_{256} F_{319}

Bold letters indicate amino acids shared between dioxins and metabolites, red letters indicate amino acids shared between DiCDD and TCDD

https://doi.org/10.1371/journal.pone.0267162.t001

primarily by G_{316}, A_{317}, T_{321}, V_{382}, $I_{386}$and L_{497}. Additionally, π-π interactions formed by $F_{125}$and F_{226} were also involved in the stabilization of each dioxin within the pCYP1A2 active site.

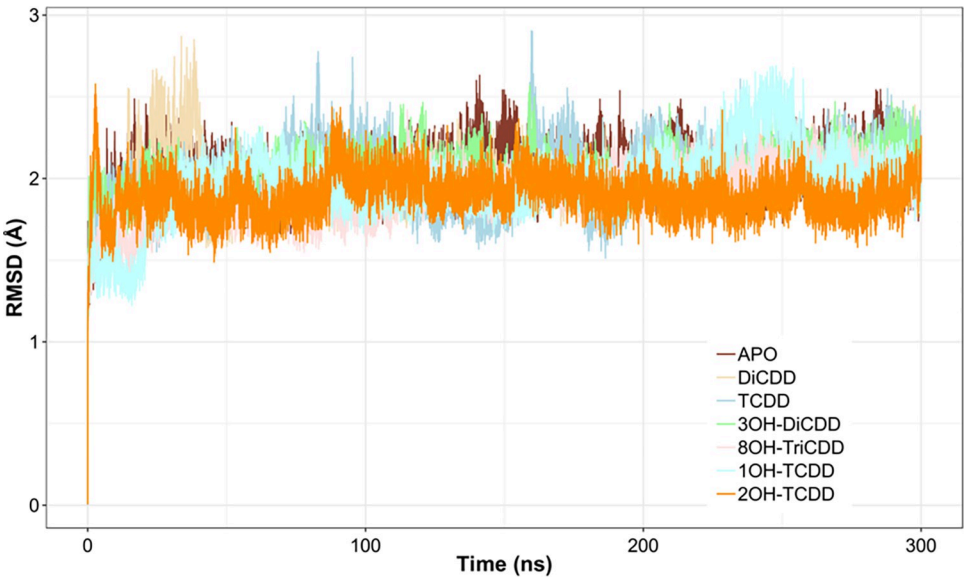

Fig 3. The root-mean-square deviation (RMSD) values collected during MD simulations of the examined dioxin-pCYP1A2 complexes (100–300 ns); APO–substrate-free form of pCYP1A2.

https://doi.org/10.1371/journal.pone.0267162.g003

The distance between the heme iron atom and the dioxin metabolite carbon atom that is nearest to the iron was calculated to assess the potential of a hydroxylated metabolite to leave the pCYP1A2 active site. The calculated distances oscillated around 5.36 ± 0.35 Å for 3OH-DiCDD, 5.71 ± 0.24 Å for 8OH-TriCDD, 6.13 ± 0.31 Å for 1OH-TCDD and 5.35± 0.37 Å for 2OH-TCDD (Fig 6). Each metabolite was stabilized primarily by G_{316} A_{317} $T_{321}$and L_{497}. Additionally, π-π interactions formed by F_{226} were also involved in the stabilization of each metabolite in the pCYP1A2 active site (Table 1, Fig 5).

2.3. Molecular dynamics simulation of PCDD-human CYP1A2 complexes

Similar to pCYP1A2, the distance between the heme oxygen atom and the dioxin carbon atom that is nearest to the oxygen was also calculated for human CYP1A2. The calculated distances oscillated around 4.15 ± 0.54 Å for DiCDD and 3.85 ± 0.34Å for TCDD (S4A and S4B Fig). In addition, the angle between the heme iron, oxygen and the dioxin carbon atom that is nearest to the oxygen oscillated around 145.45 ± 0.1˚ and 150.96 ± 0.9˚ for DiCDD and TCDD, respectively (S4C and S4D Fig).

2.4. Calculated binding affinity of the PCDD-pCYP1A2 complexes after MD simulations and thermodynamic integration

The binding free energy of the TCDD-pCYP1A2 complex (-13.671±0.020 kcal·mol^{-1}) was lower than that of the DiCDD-pCYP1A2 complex (-12.778±0.026 kcal·mol^{-1}) (Table 2). The binding free energy for DiCDD, in turn, was lower in comparison to that for 3OH-DiCDD (-9.697±0.053 kcal·mol^{-1}). Similarly, 8OH-TriCDD (-12.007 ± 0.032 kcal·mol^{-1}) showed a slightly lower affinity to the pCYP1A2 active site than TCDD. In contrast, the two other TCDD metabolites *i.e.*, 1OH-TCDD (-24.415±0.050 kcal·mol^{-1}) and 2OH-TCDD (-15.324 ±0.043 kcal·mol^{-1}) showed higher affinity to the pCYP1A2 active site than TCDD. The pCYP1A2 demonstrated higher affinity towards DiCDD and TCDD in comparison to other members of pCYP1 enzymes [12, 19] (S3 Table).

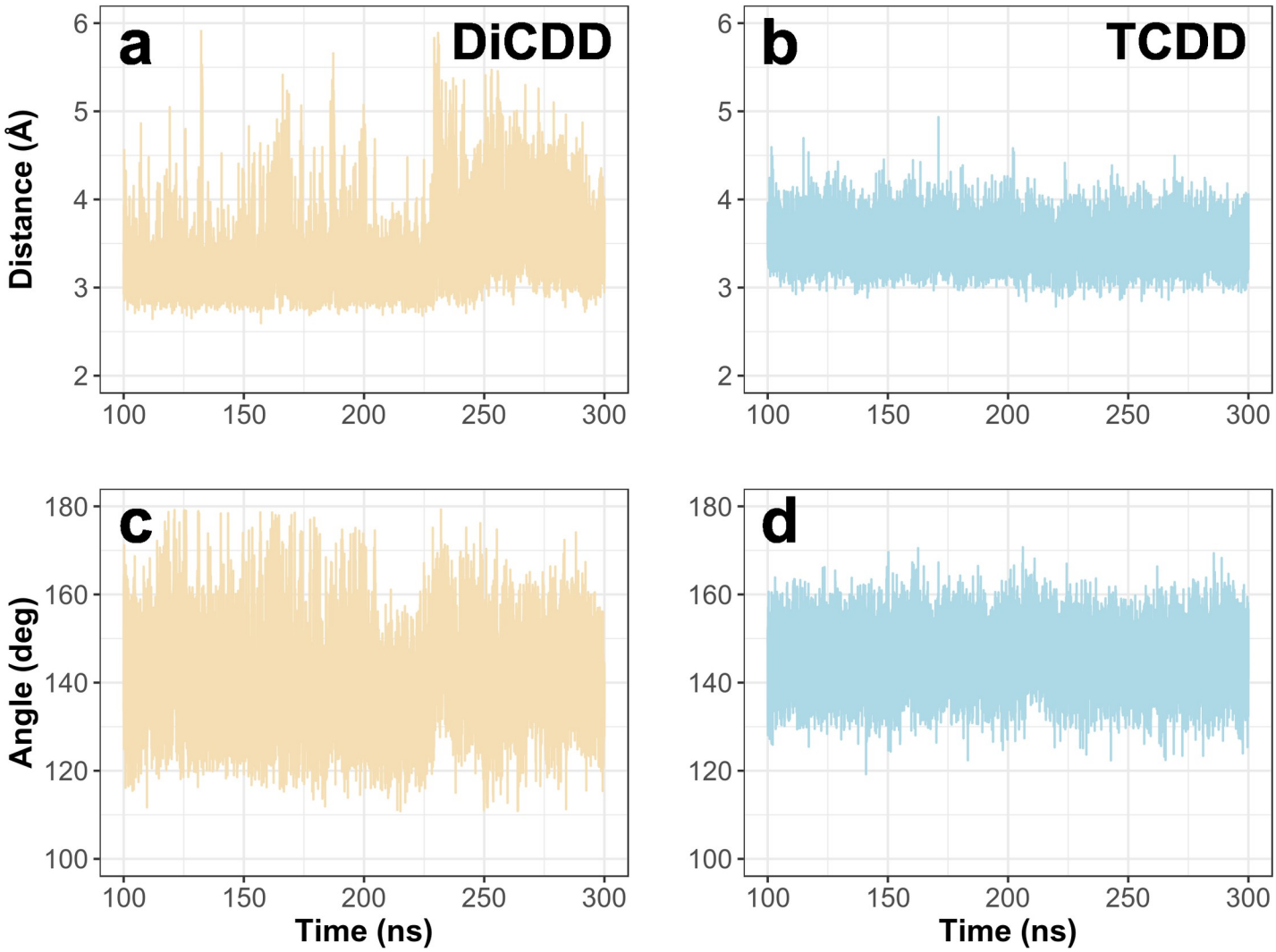

Fig 4. Time-dependent changes in the distance between the pCYP1A2 heme oxygen and the dioxin carbon atom that is nearest to the oxygen (a, b) and in the angle between the pCYP1A2 heme iron, oxygen and the dioxin carbon atom that is nearest to the oxygen (c, d).

https://doi.org/10.1371/journal.pone.0267162.g004

In addition, the binding free energy of each residue forming all the examined dioxin-pCYP1A2 complexes was analyzed to estimate the influence of particular residues on the dioxin-enzyme binding. The amino acids with the strongest impact on the formation of the dioxin-pCYP1A2 complexes are listed in Table 3 and visualized in Fig 5. The complexes were found to be stabilized by hydrophobic interactions including π-stacking interactions (F_{125} and F_{226}) between a dioxin and pCYP1A2.

2.5. Access channels of pig CYP1A2

The specific interactions of a particular dioxin with pCYP1A2 affected the opening status (open vs. closed) of the substrate channels leading to the active site of the enzyme (Fig 7). To assess the potential of pCYP1A2 to hydroxylate a dioxin, the availability of access channels were analyzed in depth. The MD simulations revealed the presence of two channels (channel 2c and 2a) that were most frequently activated (opened) upon binding the examined dioxins (Fig 7A). Therefore, the subsequent analysis was performed only with regard to these two

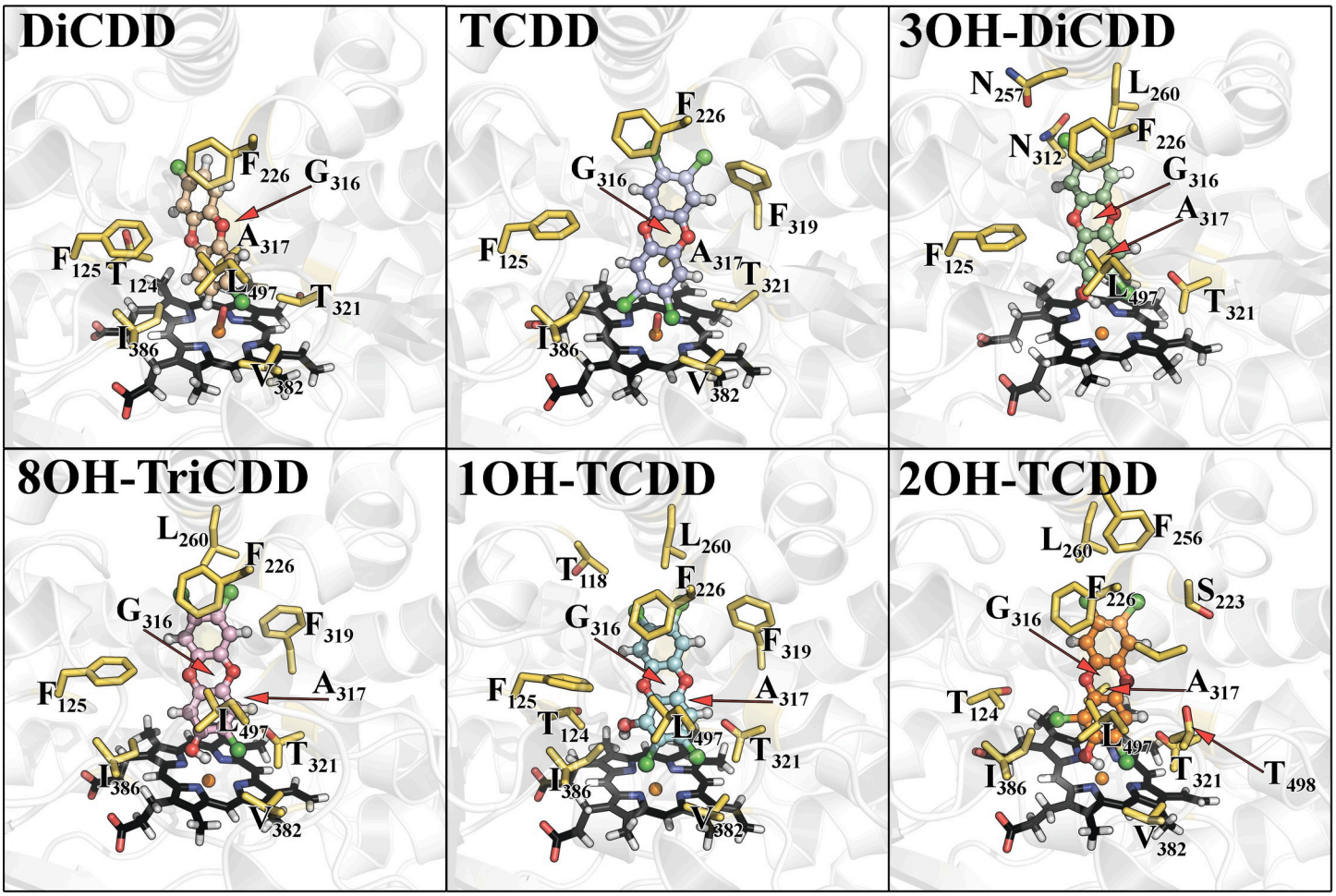

Fig 5. The visualization of a dioxin position in the active site of pCYP1A2duringmolecular dynamics simulations. Side chains of pCYP1A2 amino acids interacting with the examined dioxin are depicted in yellow; heme is black; DiCDD is beige, TCDD is lavender, 3OH-DiCDD is green, 8OH-TriCDD is pink, 1OH-TCDD is pale willow-green and 2OH-TCDD as orange.

https://doi.org/10.1371/journal.pone.0267162.g005

channels (Table 4). The accessibility of the substrate channels during the simulation time is shown in Fig 7B. In substrate-free pCYP1A2, channels 2c and 2a were open for 25.35% and 74.42% of the simulation time, respectively. Compared to the APO form of the enzyme, the presence of DiCDD or 8OH-TriCDD within the pCYP1A2 active site promoted the opening of the channel 2c for 63.30% or 35.68%, respectively. Furthermore, the binding of TCDD or its two metabolites i.e., 1OH-TCDD and 2OH-TCDD to the active site of the pCYP1A2 resulted in a closure of channel 2c (Table 4). The binding of all examined dioxins resulted in a closure of channel 2a. The presence of dioxin metabolites within the enzyme active site did not promote opening of channel S (Fig 7B).

3. Discussion

The members of the CYP1 family (CYP1A1, CYP1A2 and CYP1B1) are directly involved in biotransformation of many important endogenous and exogenous substances including steroid hormones, drugs or dioxins [21]. Previously, we have examined the potential of pig CYP1A1 [12] or CYP1B1 [19] to hydroxylate dioxins which differ in their toxicity and biodegradability. In the current study, we have investigated *in silico* the binding affinity and

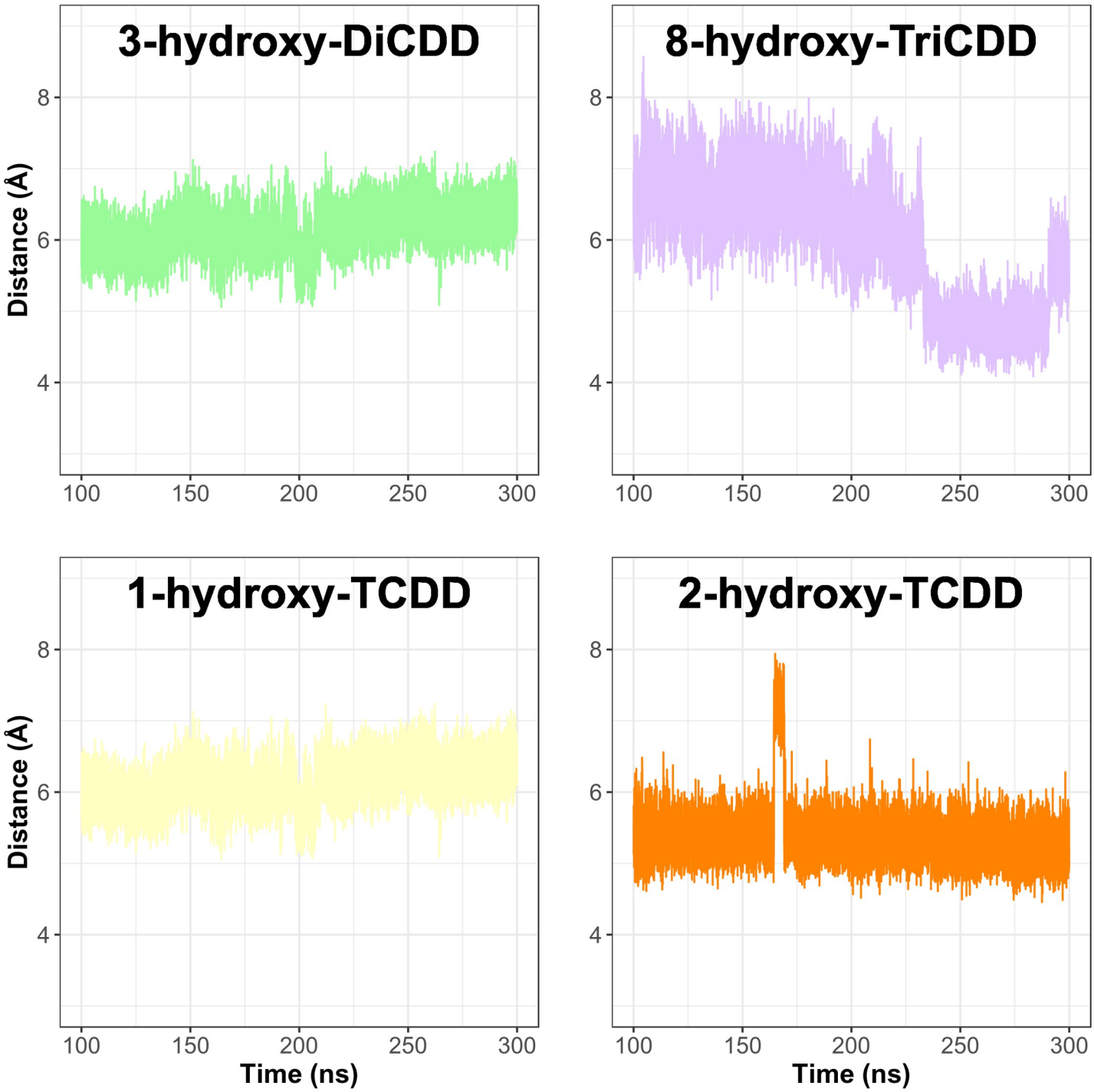

Fig 6. Time-dependent changes in the distance between the pCYP1A2 heme iron and the dioxin metabolite carbon atom that is nearest to the iron. 3OH-DiCDD– 3-hydroxy-2,7-dichlorodibenzo-*p*-dioxin, 8OH-TriCDD– 8-hydroxy-2,3,7-trichlorodibenzo-*p*-dioxin, 1OH-TCDD– 1-hydroxy-2,3,7,8-tetrachlorodibenzo-*p*-dioxin, 2OH-TCDD– 2-hydroxy-1,3,7,8-tetrachlorodibenzo-*p*-dioxin.

https://doi.org/10.1371/journal.pone.0267162.g006

selectivity between pig CYP1A2 and DiCDD–a less toxic and easily biodegraded dioxin or TCDD–a dioxin that is strongly toxic and highly resistant to biodegradation. These molecular interactions were also analyzed between pCYP1A2 and four selected dioxin metabolites:

Table 2. The absolute binding free energy (kcal·mol^{-1}) calculated through MD simulations and thermodynamic integration for the dioxin-pCYP1A2 complexes.

Energy component	DiCDD	3OH-DiCDD	TCDD	8OH-TriCDD	1OH-TCDD	2OH-TCDD
$\Delta G^{prot}_{elec+vdw+rest}$	-22.369±0.022	-21.939±0.051	-23.335±0.013	-23.825±0.027	-37.629±0.045	-28.110±0.040
$\Delta G^{solv}_{elec+vdw}$	2.611±0.014	5.077±0.016	2.497±0.016	4.996±0.017	6.423±0.021	5.822±0.016
ΔG^{solv}_{rest}	6.980	7.165	6.894	6.936	6.791	6.964
$\Delta G^{0}_{binding}$	**-12.778±0.026**	**-9.697±0.053**	**-13.671±0.020**	**-12.007±0.032**	**-24.415±0.050**	**-15.324±0.043**

$\Delta G^{prot}_{elec+vdw+rest}$–ligand decoupling from complex; $\Delta G^{solv}_{elec+vdw}$–ligand decoupling from solution; ΔG^{solv}_{rest}–ligand restraints added to decoupled ligand; $\Delta G^{0}_{binding}$–absolute binding free energy, $\Delta G^{o}_{binding} = \Delta G^{prot}_{elec+vdw+rest} + \Delta G^{solv}_{elec+vdw} + \Delta G^{solv}_{rest}$

DiCDD– 2,7-dichlorodibenzo-*p*-dioxin, TCDD– 2,3,7,8-tetrachlorodibenzo-*p*-dioxin, 3OH-DiCDD– 2,7-dichloro-3-hydroxy-dibenzo-*p*-dioxin
8OH-TriCDD– 2,3,7-trichloro-8-hydroxy-dibenzo-*p*-dioxin, 1OH-TCDD– 2,3,7,8-tetrachloro-1-hydroxy-dibenzo-*p*-dioxin, 2OH-TCDD– 1,3,7,8-tetrachloro-2-hydroxy-dibenzo-*p*-dioxin

https://doi.org/10.1371/journal.pone.0267162.t002

3OH-DiCDD, 1OH-TCDD, 2OH-TCDD and 8OH-TriCDD [11, 14, 26]. Moreover, we have studied the availability of access channels within the pCYP1A2 molecule after dioxin binding to analyze the potential routes of the entrance of the ligands and the exit of the hydroxylated products.

The concept of CYP-mediated metabolism of TCDD relies entirely upon the research reporting the formation of the dioxin metabolites in human and animal tissues [14, 24, 27] and/or the presence of catalytic activity of CYP1 enzymes towards TCDD [11, 25]. The presence of TCDD metabolites–as well as those of other dioxins–was detected in human faeces, blood serum and urine as well as in body fluids of mice and dogs [14, 24, 27]. Moreover, despite the documented formation of TCDD metabolites, the reason for slow and non-efficient degradation of this dioxin is still unknown.

The CYP-mediated hydroxylation process of dioxins is initiated by an effective binding of a specific substrate. The binding free energy reflects the binding affinity–the lower the energy, the higher the affinity. The results of the current study demonstrated that binding free energy of the TCDD-pCYP1A2 complex was lower than that of the DiCDD-pCYP1A2 complex, suggesting that TCDD is held stronger within the active site of CYP1A2. Several studies demonstrated a growing ligand binding affinity accompanying successive substituting the ligand molecule with chlorine atoms [28–30].

The binding specificity data demonstrated that the examined dioxins were stabilized within the CYP1A2 active site mostly *via* hydrophobic interactions. Among these, the π-stacking

Table 3. The relative binding free energy (ΔΔG;kcal·mol^{-1}) calculated for individual amino acids stabilizing the dioxin-pCYP1A2 complexes.

Dioxin	$F_{125}A$	$F_{226}A$	$G_{316}A$	$A_{317}G$	$T_{321}A$	$V_{382}A$	$I_{386}A$	$L_{497}A$
DiCDD	1.527±0.033	2.202±0.015	0.615±0.003	0.990±0.101	1.122±0.012	0.897±0.008	1.131±0.014	2.910±0.017
3OH-DiCDD	–	-0.344±0.027	-0.248±0.004	1.303±0.004	1.776±0.014	–	–	2.960±0.034
TCDD	0.807±0.031	2.010±0.012	0.091±0.004	0.471±0.004	0.960±0.007	-0.040±0.007	0.388±0.009	3.508±0.013
8OH-TriCDD	–	-0.322±0.021	-0.386±0.003	0.745±0.004	0.270±0.07	–	–	4.443±0.031
1OH-TCDD	–	-0.039±0.024	0.747±0.004	0.142±0.004	1.761±0.08	–	–	2.612±0.032
2OH-TCDD	–	2.416±0.024	1.530±0.004	1.130±0.003	-0.087±0.009	–	–	3.354±0.024

DiCDD– 2,7-dichlorodibenzo-*p*-dioxin, TCDD– 2,3,7,8-tetrachlorodibenzo-*p*-dioxin, 3OH-DiCDD– 2,7-dichloro-3-hydroxy-dibenzo-*p*-dioxin
8OH-TriCDD– 2,3,7-trichloro-8-hydroxy-dibenzo-*p*-dioxin, 1OH-TCDD– 2,3,7,8-tetrachloro-1-hydroxy-dibenzo-*p*-dioxin, 2OH-TCDD– 1,3,7,8-tetrachloro-2-hydroxy-dibenzo-*p*-dioxin
The value for wild type of the pCYP1A2 bound DiCDD or TCDD was used as a reference (ΔG = 0)

https://doi.org/10.1371/journal.pone.0267162.t003

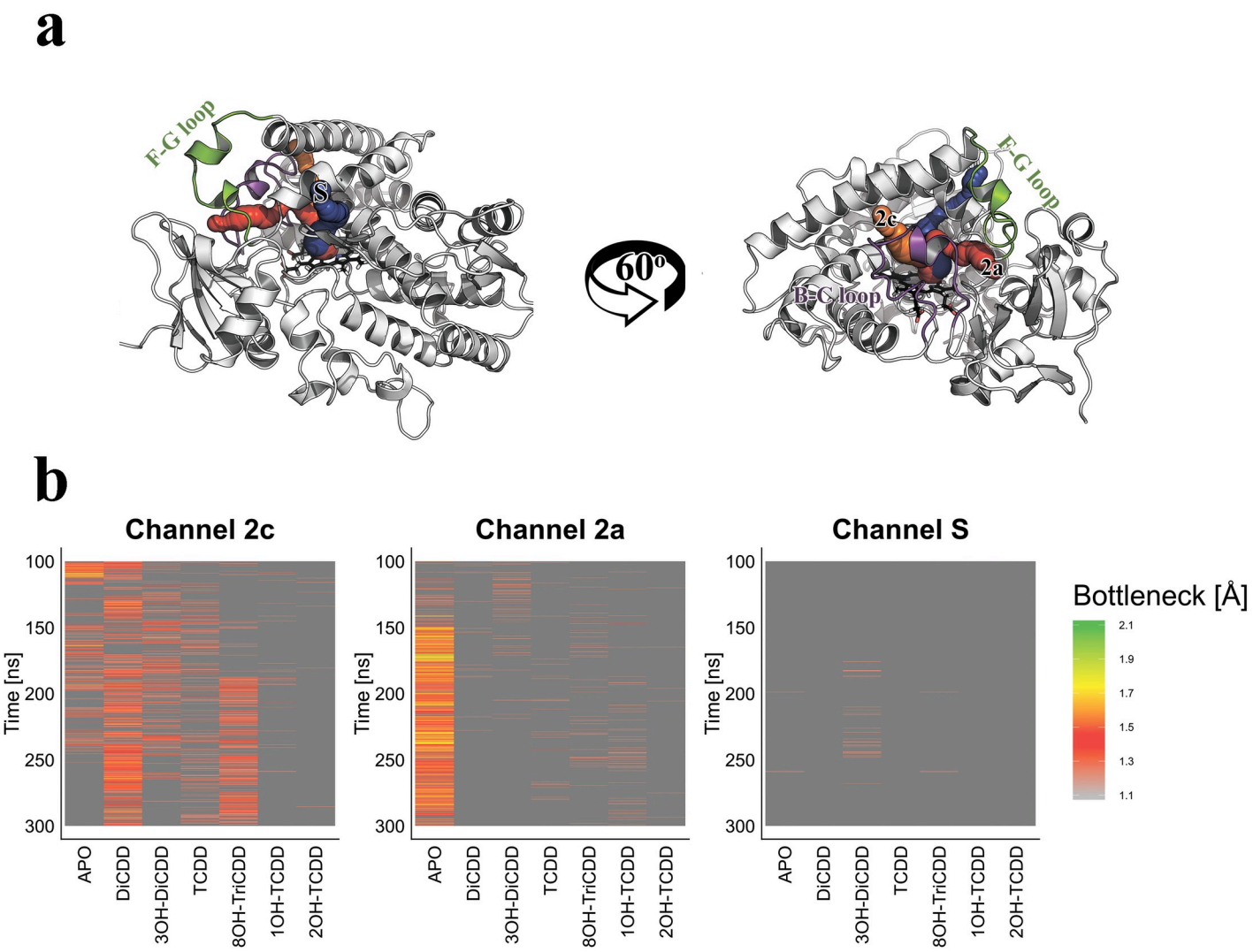

Fig 7. The access channels of the pCYP1A2 molecule shown in two different spatial enzyme orientations (a). Channel S is depicted in blue, channel 2c in orange, channel 2a in red and the heme molecule is shown in black. The F-G (green) and B-C (violet) loops are of particular importance for the state of the channel (open *vs*. closed). Dioxin-induced changes in the availability of the access channels identified within the pCYP1A2 molecule (b); Apo–substrate free form of pCYP1A2.

https://doi.org/10.1371/journal.pone.0267162.g007

interactions, formed by F_{115}or F_{226}, seem to play an important role in the stabilization of a dioxin in the enzyme catalytic site. In addition, it was demonstrated that all examined dioxins assumed the same plane orientation within the CYP1A2 active site. The incorporation of hydroxyl group to the substrate is the first step of dioxin biodegradation catalyzed by CYP1 enzymes [9, 11]. The efficiency of the hydroxylation depends on the distance between the oxygen atom of the CYP1A2's heme and the nearest carbon atom of the dioxin [31]. (It was suggested by Lonsdale et al. [32] that the distance between the CpdI oxygen and the ligand should range within 3-5Å to enable hydroxylation to occur. The distances between the oxygen atom of the enzyme's heme and a particular dioxin (DiCDD or TCDD) oscillated around 3–3.5Å. Such a small distance implies the potential of being hydroxylated by pCYP1A2. Similar results were obtained for hCYP1A2 (S4 Fig). On the other hand, the values of measured angles between CYP1A2 and DiCDD or TCDD exceeded the values described by Lonsdale et al. [32] as being effective in incorporating a hydroxyl group into the aromatic ring. Moreover, apart

Table 4. The features of the two most accessible access channels of pCYP1A2.

Name	Availability of the channel[a]	Mean bottleneck radius (Å)	Maximal bottleneck radius (Å)	Mean pathway length (Å)
Channel 2c				
APO	25.35%	1.35±0.13	1.87	23.95
DiCDD	63.30%	1.35±0.12	1.85	23.67
3OH-DiCDD	26.80%	1.31±0.09	1.70	22.71
TCDD	19.60%	1.28±0.07	1.57	23.07
8OH-TriCDD	35.68%	1.31±0.08	1.64	24.93
1OH-TCDD	2.03%	1.28±0.08	1.55	26.25
2OH-TCDD	1.00%	1.26±0.07	1.50	26.47
Channel 2a				
APO	74.42%	1.48±0.15	2.07	23.22
DiCDD	0.13%	1.24±0.03	1.32	30.37
3OH-DiCDD	5.45%	1.27±0.06	1.53	28.45
TCDD	1.95%	1.25±0.05	1.44	29.18
8OH-TriCDD	4.35%	1.25±0.05	1.44	28.32
1OH-TCDD	5.08%	1.26±0.06	1.48	25.38
2OH-TCDD	0.62%	1.23±0.03	1.32	26.58

https://doi.org/10.1371/journal.pone.0267162.t004

from the enzyme's hydroxylating potential, the successful biodegradation of dioxins also requires an effective evacuation of the polar product from the active site [20, 33]. We found that access channels S and 2a remained closed during the MD simulation of the two dioxins, while the 2c channel was opened only by DiCDD. The results suggest that after binding, both dioxins remain locked within the CYP1A2 active site, making hydroxylation impossible to proceed and also blocking the enzyme for other ligands. Moreover, the sequestration of TCDD within the pCYP1A2 may foreclose the dioxin molecule from being detoxified by other enzymes, which may be partially responsible for high toxicity of TCDD [24].

Analysis of binding free energy revealed that pCYP1A2 demonstrated the highest affinity towards both DiCDD and TCDD compared to previously analyzed pCYP1 enzymes (S3 Table; [12, 19]). The measured distances of DiCDD or TCDD from CYP1A2 heme's oxygen atom were smaller than in CYP1A1 or CYP1B1, reflecting higher potential of being hydroxylated by the enzyme and suggesting a greater contribution of CYP1A2 to dioxin biodegradation. This assumption seems to be supported by the hepatic localization of pig CYP1A2 [21, 22, 34]. Some interesting differences were also noted in the behavior of the substrate channels after dioxin binding to different CYP1 molecules. Binding of DiCDD or TCDD to CYP1A2 resulted in a rapid closure of channel 2a, and channel S remained closed through the entire simulation time. In CYP1A1, the binding of TCDD resulted in channel S closure, however channel S remained open after binding DiCDD (S5 Fig; [12]). Similarly, both dioxins opened channel S after binding to CYP1B1 (S6 Fig; [19]). This seems particularly important since channel S is considered to be an exit channel from the enzyme's active site. It cannot be excluded that the unavailability of channel S overcomes the impact of favorable affinity and the hydroxylating potential, and results in the ineffective biodegradation of TCDD by CYP1A2.

A few studies reported the formation of primary metabolites of TCDD in animal organisms as an indication of their biodegradation [25–27]. No research, however, demonstrated the occurrence of further stages of biodegradation or provided any reliable reasons for the lack of TCDD detoxification. In the current study, we analyzed molecular interactions between CYP1A2 and four dioxin metabolites. 3OH-DiCDD, a primary metabolite of DiCDD [11] and 8OH-TriCDD, a TCDD metabolite [14] showed a lower affinity to CYP1A2 than the respective

original dioxin. However, the remaining TCDD metabolites *i.e.*, 1OH-TCDD [26] and 2OH-TCDD [14] showed higher affinity to the pCYP1A2 active site than TCDD. Interestingly, the molecules of the two latter metabolites have more chlorine atoms than 8OH-TriCDD or 3OH-DiCDD. Numerous studies demonstrated that the increase in the binding affinity was accompanied by the greater number of chlorine atoms [28, 30]. To determine the probability of a hydroxylated product to be released from the active site, the distances between the iron atom of the heme and a particular dioxin metabolite were estimated. It should be emphasized that all calculated distances exceeded 5 Å (5.35–6.13 Å), strongly suggesting that the hydroxylated metabolites should not remain within the CYP1A2 active site [32]. The analysis of access channels revealed that channel 2c was opened only by 8OH-TriCDD. None of the metabolites bound to CYP1A2 promoted the opening of channel S. Contrary to the distances between the metabolites and the pCYP1A2 active site, the channel data suggest that the hydroxylated products are probably not capable of leaving the active site, which results in the blockage of the enzyme.

The active sites of pCYP1A2, CYP1A1 and CYP1B1formed by 12 canonical α-helices and 6 β-sheets were demonstrated to be deeply buried in the CYP molecule (the current study; [12, 19]). Similar to other CYP1 enzymes, the analysis of pCYP1A2 active site demonstrated the presence of a narrow and planar active site embedded in the enzyme molecule. The cavity volume of the CYP1A2 active site was close to that of CYP1A1 and considerably bigger than that of CYP1B1. The size and specific shape of the CYP1 active site affects hydroxylation of hydrophobic and planar compounds like PCDDs [11, 12]. The results of our previous study demonstrated, that smaller active site may result in the immobilization of a ligand, forcing a certain spatial orientation which may inhibit hydroxylation [19]. It is suggested, that enlarging the binding pocket through mutagenesis-derived specific changes in amino acids forming the helices of the enzyme's active site, may ease TCDD biodegradation [9]. In summary, pCYP1A2 demonstrated the highest affinity towards both DiCDD and TCDD compared to other members of the pCYP1 family. Similar to the pCYP1A1 or pCYP1B1, all dioxin-pCYP1A2 complexes were found to be stabilized by hydrophobic interactions including π-stacking interactions. The distances between the heme oxygen atom and the dioxin carbon atom that is nearest to the oxygen indicated high hydroxylating potential of the enzyme–higher than those of other pCYP1 enzymes. Also, the distances from the heme iron atom did not suggest difficulties with metabolite egressing the active site. However, we also demonstrated that the binding of all dioxins resulted in a closure of access channel 2a, and the presence of metabolites did not promote opening of exit channel S. It is possible that such behavior of pCYP1A2 substrate channels overcomes the impact of the favorable affinity and hydroxylating potential of the enzyme, and results in the ineffective biodegradation of TCDD by CYP1A2.The presented data partially explain the molecular mechanisms underlying the slow and non-efficient degradation of TCDD by CYP enzymes. Although the results of the current study shed some light on the matter of CYP-mediated dioxin biodegradation, there are still more questions than answers.

4. Materials & methods

All stages of the study were performed for two dioxin congeners, characterized by distinctively different toxicity and susceptibility to biodegradation, i.e., DiCDD–less toxic and easily degraded, and TCDD–highly toxic and resistant to biodegradation. We also examined four dioxin metabolites: 3OH-DiCDD, 8OH-TriCDD, 1OH-TCDD and 2OH-TCDD. Chemical formulas of both dioxins and their metabolites are presented in Fig 8. Porcine *CYP1A2* cDNA sequence was established experimentally by next generation sequencing (NGS; [6]). In our

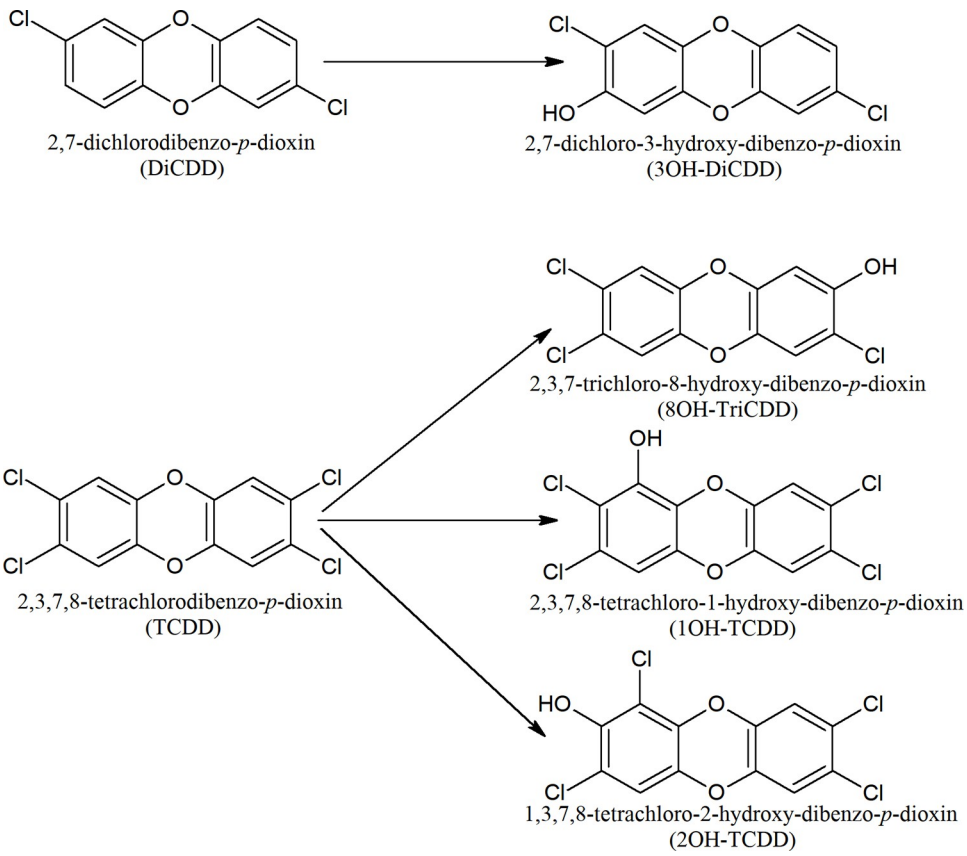

Fig 8. Chemical formulae of DiCDD and TCDD as well as their potential metabolites.

https://doi.org/10.1371/journal.pone.0267162.g008

previous experiment, total RNA was isolated from porcine liver and tested for concentration, quality and integrity. Next, cDNA strands were synthesized and DNA libraries were amplified and quantified. Finally, libraries were sequenced on llumina HiSeq2500 high throughput sequencing instrument (OpenExome, Poland) with 100 paired-end (PE) sequencing [6]. The porcine *CYP1A2* (pCYP1A2) sequence was localized in the transcriptome, trimmed and submitted to GenBank under the following accession number: AIY35109.1. The nucleotide (nt) sequence was then translated to amino acid (aa) sequence.

4.1. Homology modeling of the pCYP1A2 catalytic domain

The amino acid sequence of pCYP1A2 protein was used to perform homology modeling of the enzyme catalytic domain (aa 34–516). The crystalline structure of human CYP1A2 (PDB ID: 2HI4) was chosen as a template. The sequence alignment between pCYP1A2 and the template was performed with the use of MUSCLE software [35]. A tertiary structure of pCYP1A2 was generated using Modeller 9v14 software [36]. Models with the lowest Discrete Optimized Protein Energy (DOPE) score were selected for further analysis. The reliability of the constructed models was evaluated with the use of PROCHECK, ProSA-web and VERIFY3D [37–40]. The model with the best validation scores was selected to be further analyzed. The cavity volume of the pCYP1A2 active site was calculated using VOIDOO software [41]. The analysis was carried out with the probe-occupied algorithm. The probe radius and primary grid spacing were set to 1.4 Å and 0.33 Å, respectively. Other calculation parameters were set to default values.

4.2. Molecular docking of dioxins to the pCYP1A2 active site

Spatial structures of the two selected dioxin congeners (DiCDD and TCDD) and their metabolites (8OH-TriCDD, 3OH-DiCDD,2OH-TCDD,1OH-TCDD) were obtained from ZINC database [42]. Prior to dioxin docking, hydrogen atoms and charges were added to the modeled structure of pCYP1A2 with the use of MGL Tools 1.5.4 [43]. The parameters of the ferric heme were applied [44]. The molecular docking was performed using AutoDock Vina 1.1.2 program [45]. The grid box was constructed around the active site of pCYP1A2 protein with X, Y, Z parameters set to 15, 15 and 15 Å. The docking analysis was performed with exhaustiveness of 32. Other parameters were set to default values. The program generated 20 results reflecting the best spatial positions of a dioxin molecule within the pCYP1A2 active site. For each dioxin, the complex with the lowest energetic binding score was chosen as the most energetically favorable, and was used to perform the subsequent molecular dynamics (MD) simulation. To confirm the high reliability of the constructed homology model of porcine CYP1A2, a corresponding analysis was performed for the crystalline structure of human CYP1A2 (PDB ID: 2HI4).

4.3. Molecular dynamics simulation of the PCDD-pCYP1A2 complexes

Molecular dynamics simulations were carried out with GROMACS 4.6.7 software using ffamber99sb force field [46, 47]. The heme parameters were applied following [44], using the heme Compound I intermediate (CpdI). To obtain force fields of the examined dioxins, the spatial geometry of their structure was optimized with the use of Gaussian 09 software, applying B3LYP/6-31G(d) level of theory [48]. Afterwards, the partial charges were obtained by the restrained electrostatic potential fitting technique (RESP) based on electrostatic potentials (Gaussian 09 software) and applying Hartree-Fock (HF) SCF/6-31G(d) level of theory [49]. For MD simulation, a rhombic dodecahedron box of explicit TIP3P water molecules was constructed around the examined complexes in a 10 Å distance from every peripheral residue. Sodium and chlorine ions were added to neutralize the system [50].

Each PCDD-pCYP1A2 complex was relaxed using a harmonic constant of 1000 $J \cdot mol^{-1} \cdot nm^{-1}$ with restraints on protein heavy atoms. The energy minimization was conducted with the steepest-descent algorithm through 5000 steps. The system was first heated from 0 to 300 K for 500 ps under NVT (constant number of particles, volume and temperature) conditions. Next, the system was equilibrated under NPT (constant number of particles, pressure and temperature) conditions for 1 ns. The relaxed dioxin-pCYP1A2 complexes underwent a 300 ns MD simulation under NPT conditions. Periodic boundary conditions and 12 Å cut-off for non-bonded van der Waals (vdW) interactions were applied. Particle Mesh Ewald (PME) algorithm was used to calculate the long-range electrostatic interactions between atoms. All bonds involving hydrogen atoms were constrained by LINCS algorithm [51]. The time step for MD simulation was set to 2 fs. In addition, MD simulation of the substrate-free form (APO) of porcine CYP1A2 was performed to exclude the effect of substrate binding on protein structure.

4.4. Binding free energy of the PCDD-pCYP1A2 complexes

In the present study we used two different methods to predict binding free energy, i.e., absolute binding free energy (ABF) and thermodynamic integration (TI). ABF was employed to estimate the binding affinity of dioxin molecules to the pCYP1A2 active site [52]. TI was used to determine the impact of selected aa residues on a dioxin stabilization within the pCYP1A2 active site [53].

4.4.1. Absolute binding free energy. Calculations of ABF for the PCDD-CYP1A2 complexes were performed with the use of a non-physical thermodynamic cycle depicted in S7 Fig.

Two systems were analyzed in the cycle in the presence of water molecules: 1/ PCDD molecule was bound to the active site of pCYP1A2 and 2/ unbound PCDD molecule. To estimate the ABF between a PCDD and the pCYP1A2 active site, the ligand van der Waals and electrostatic interactions were decoupled ($\Delta\lambda = 0.05$) and annihilated ($\Delta\lambda = 0.1$), respectively (S7 Fig, A→B). Next, the relative position and orientation of the PCDD bound to the pCYP1A2 were restrained by harmonic potential using a harmonic constant (4184.0J·mol^{-1}·nm^{-1}for distances; 41.84 J·mol^{-1}·nm^{-1}for angles). These restraints were executed by twelve non-uniformly distributed λ states ranged from 0 to 1 (0.000, 0.010, 0.025, 0.050, 0.075, 0.100, 0.150, 0.200, 0.300, 0.500, 0.750, 1.000). The relaxation of the systems for each λ-state was performed as described in Section 2.3 (*Molecular dynamics simulation of the PCDD-pCYP1A2 complexes*) with the use of GROMACS 5.1.4. Calculations of ABF were performed during 40 ns with a 2 fs time-step. A soft-core potential was employed to improve the transformation of van der Waals interactions. Particle Mesh Ewald (PME) algorithm was used to calculate the long-range electrostatic interactions between atoms. All bonds involving hydrogen atoms were constrained by P-LINCS algorithm. The g_bar tool (GROMACS package) implementing the Bennet's acceptance ratio method (BAR) was used to estimate the ABF of PCDD bound to the pCYP1A2 active site. To reach an equilibrium, the first 10 ns of each simulation was discarded.

4.4.2. Thermodynamic integration. To determine the impact of selected aa residues on a dioxin stabilization within the pCYP1A2 active site, the residues were mutated during TI calculation. Calculations of binding free energy for PCDD-pCYP1A2 complexes were performed with the use of the thermodynamic cycle depicted in S2 Fig. The residues important for a dioxin stabilization within the enzyme active site (wild-type; WT) were designated for mutation (Mut) following the MD simulations. Briefly, the difference in binding free energy between aPCDD-pCYP1A2$_{WT}$ complex and aPCDD-pCYP1A2$_{MUT}$ complex was estimated on the basis of an alchemical transformation with the use of λ parameter coupling. The total energy of each state is described by its Hamiltonian (H) i.e., H0 and H1 for thePCDD-pCYP1A2$_{WT}$ complex and thePCDD-pCYP1A2$_{MUT}$ complex, respectively. The transformation between the two states is described by adding the λ parameter to the H. The intermediate values of the λ parameter represent intermediate states of the transformation. The integration of the free energy values along a continuous path connecting the initial (H0) and final (H1) state was used to estimate the difference in binding free energy as follows:

$$\Delta G_{binding}(A \rightarrow B) = \int_0^1 \langle \frac{\delta H(q,p,\lambda)}{\delta \lambda} \rangle_\lambda d\lambda$$

where, q stands for the atomic position, p stands for the linear momentum, and the angular bracket stands for a Boltzmann-weighted ensemble average at a particular λ value. The difference in the relative binding free energy (ΔΔG) between the PCDD-pCYP1A2$_{WT}$ complex and the PCDD-pCYP1A2$_{MUT}$ complex can be calculated with the use of a thermodynamic cycle (S8 Fig). Based on the cycle, the ΔΔG can be calculated according to the following equation:

$$\Delta\Delta G_{(WT \rightarrow Mut)} = \Delta G_{binding}(WT) - \Delta G_{binding}(Mut) = \Delta G_{bound(WT \rightarrow Mut)} + \Delta G_{unbound(WT \rightarrow Mut)}$$

where, $\Delta G_{bound(WT \rightarrow Mut)}$ stands for alchemical transformation of the ligand-bound form ofwild-type pCYP1A2 to the mutated pCYP1A2, $\Delta G_{unbound(WT \rightarrow Mut)}$ represents alchemical transformation of the ligand free-form of wild-type the pCYP1A2 to the mutated pCYP1A2 protein.

For calculation of ΔΔG, the wild-type of pCYP1A2 was used as a reference. Two systems were analyzed in the cycle in the presence of water molecules: 1/ a PCDD molecule bound to the active site of pCYP1A2 and 2/ ligand-free form of the pCYP1A2 protein; thirty λ-states were established in each system. The relaxation of the complexes for each λ-state was

performed as described in Section 2.3 (*Molecular dynamics simulation of the PCDD-pCYP1A2 complexes*). The free energy calculation was performed during 30 ns with the use of Hamiltonian replica exchange dynamics with a 2 fs time-step. According to the Gibbs sampling scheme, 3 million swaps between any state pair were performed for every 1000 time steps. The g_bar tool (GROMACS package) implementing the Bennet's acceptance ratio method (BAR) was used to estimate the difference in relative binding free energy (ΔΔG) between wild-type and mutant pCYP1A2 protein bound TCDD or DiCDD within the enzyme active site. To reach equilibrium, the first 10 ns of each simulation was discarded. These differences reflect the importance of particular residues in dioxin stabilization. The obtained positive/negative values denote that the interactions between the substituted residues and a dioxin were weaker/stronger, respectively, than those of the corresponding "wild type" residues.

4.5. Access channels analysis

Access channels of pCYP1A2 molecule were analyzed using CAVER 3.0.1 software [54]. The snapshots of MD simulation trajectories of the dioxin-pCYP1A2 complexes as well as the unbound CYP1A2 were extracted at every 50 ps from 100 to 300 ns. The probe radius and clustering threshold of each channel were set to 1.2 Å and 3.5 Å, respectively. Default settings for other parameters were used throughout the calculations. The beginning of each channel was localized 3 Å above the iron atom of the heme molecule. The tunnels were visualized with the use of PyMOL software [55]. To extend the knowledge concerning a potential ability of porcine CYP1A2 enzyme to hydroxylate a dioxin molecule, a corresponding analysis was performed for dioxin metabolites bound within the enzyme active site.

Supporting information

S1 Table. The protein sequence identity between the CYP1A2 of the pig and other species.
(XLSX)

S2 Table. The average root-mean-square deviation (RMSD) values for the examined dioxin-CYP1A2 complexes during MD simulations.
(DOCX)

S3 Table. The absolute binding free energy (kcal·mol^{-1}) calculated for the PCDD-CYP1 complexes.
(DOCX)

S1 Fig. The amino acid sequence alignment between catalytic domains of porcine CYP1A2 and human CYP1A2 templates. Yellow background and red or black letters indicate that the sequence homology is high, medium or low, respectively. Spirals represent α-helices, arrows represent β-strands, blue stars indicate amino acids involved in the ligand binding to the enzyme active site.
(TIF)

S2 Fig. Ramachandran plot for the generated homology-based model of pCYP1A2.
(TIF)

S3 Fig. The visualization of a dioxin position in the active site of pCYP1A2 after molecular docking. Side chains of pCYP1A2 amino acids interacting with each of the examined dioxin are depicted in yellow; heme is black; DiCDD is beige, TCDD is lavender, 3OH-DiCDD is green, 8OH-TriCDD is pale pink, 1OH-TCDD is pale willow-green and 2OH-TCDD as orange.
(TIF)

S4 Fig. Time-dependent changes in the distance between the hCYP1A2 heme oxygen and the dioxin carbon atom that is nearest to the oxygen (a, b) and in the angle between the hCYP1A2 heme iron, oxygen and the dioxin carbon atom that is nearest to the oxygen (c, d).
(TIF)

S5 Fig. Dioxin-induced changes in the availability of the access channels identified within the pCYP1A1 molecule; APO–substrate free form of pCYP1A1.
(TIF)

S6 Fig. Dioxin-induced changes in the availability of the access channels identified within the pCYP1B1 molecule; APO–substrate free form of pCYP1B1.
(TIF)

S7 Fig. The thermodynamic cycle used to estimate the absolute binding free energy of a dioxin bound to pCYP1A2. Ligand of the pCYP1A2 is shown either as bound to the active site of the enzyme (right panel) or unbound (left panel) in the environment of water molecules (bluish background). A) The PCDD molecule (blue), fully able to interact with water molecules is alchemically transformed into B) non-interacting molecule (white). This transformation ($\Delta G^{solv}_{elec+vdw}$) was conducted with a series of simulations in which electrostatic (*elec*) and van der Waals (*vdw*) interactions between the ligand and water molecules are scaled to zero. C) Next, a non-interacting PCDD molecule was restrained (red pin). This transformation (ΔG^{solv}_{rest}) led to the state which is equivalent to D) non-interacting PCDD molecule restrained within the pCYP1A2 active site. E) Then, the *elec* and *vdw* interactions of the restrained PCDD molecule bound to the pCYP1A2 active site were gradually reinstated ($\Delta G^{prot}_{elec+vdw}$).F) Finally, the positional restraints of PCDD molecule bound to the pCYP1A2 active site were removed, and the unrestrained dioxin is fully able to interact with the enzyme (ΔG^{prot}_{rest}).
(TIF)

S8 Fig. The thermodynamic cycle used to determine the impact of particular amino acid residues on dioxin stabilization within the pCYP1A2 active site.
(TIF)

Author Contributions

Conceptualization: Sylwia Swigonska.

Data curation: Sylwia Swigonska.

Formal analysis: Tomasz Molcan, Anna Nynca.

Funding acquisition: Tomasz Molcan, Renata E. Ciereszko.

Investigation: Sylwia Swigonska.

Methodology: Sylwia Swigonska, Tomasz Molcan.

Project administration: Renata E. Ciereszko.

Software: Tomasz Molcan.

Supervision: Sylwia Swigonska.

Validation: Sylwia Swigonska.

Visualization: Sylwia Swigonska.

Writing – original draft: Sylwia Swigonska, Tomasz Molcan, Anna Nynca, Renata E. Ciereszko.

Writing – review & editing: Sylwia Swigonska, Anna Nynca, Renata E. Ciereszko.

References

1. Shibamoto T, Yasuhara A, Katami T. 2007 Dioxin formation from waste incineration, Rev. Environ. Contam. Toxicol. 190: 1–41. https://doi.org/10.1007/978-0-387-36903-7_1 PMID: 17432330
2. Mandal PK. 2005 Dioxin: a review of its environmental effects and its aryl hydrocarbon receptor biology, J. Comp. Physiol. B 175: 221–230. https://doi.org/10.1007/s00360-005-0483-3 PMID: 15900503
3. Petroff BK, Gao X, Rozman KK, Terranova PF. 2001 The effects of 2,3,7,8-tetrachlorodibenzo-p-dioxin (TCDD) on weight gain and hepatic ethoxyresorufin-o-deethylase (EROD) induction vary with ovarian hormonal status in the immature gonadotropin-primed rat model. Reprod. Toxicol. 15 (3): 269–274. https://doi.org/10.1016/s0890-6238(01)00132-0 PMID: 11390171
4. Grochowalski A, Chrzaszcz R, Pieklo R, Gregoraszczuk EL. 2001 Estrogenic and antiestrogenic effect of in vitro treatment of follicular cells with 2,3,7,8-tetrachlorodibenzo-p-dioxin, Chemosphere. 43: 823–827. https://doi.org/10.1016/s0045-6535(00)00440-9 PMID: 11372872
5. Morán FM, Conley AJ, Corbin CJ, Enan E, VandeVoort C, Overstreet JW, et al. 2000 2,3,7,8-tetrachlorodibenzo-p-dioxin decreases estradiol production without altering the enzyme activity of cytochrome P450 aromatase of human luteinized granulosa cells in vitro, Biol. Reprod. 62: 1102–1108. https://doi.org/10.1095/biolreprod62.4.1102 PMID: 10727284
6. Sadowska A, Nynca A, Ruszkowska M, Paukszto L, Myszczynski K, Orlowska K, et al. 2017 Transcriptional profiling of porcine granulosa cells exposed to 2,3,7,8-tetrachlorodibenzo-p-dioxin, Chemosphere. 178: 368–377. https://doi.org/10.1016/j.chemosphere.2017.03.055 PMID: 28340459
7. Nynca A, Sadowska A, Paukszto L, Molcan T, Ruszkowska M, Swigonska S, et al. 2019 Temporal changes in the transcriptomic profile of granulosa cells of pigs treated with 2,3,7,8-tetrachlorodibenzo-p-dioxin. Anim. Reprod. Sci. 207: 83–94. https://doi.org/10.1016/j.anireprosci.2019.06.007 PMID: 31213330
8. Denison MS, Soshilov AA, He G, DeGroot DE, Zhao B. 2011 Exactly the same but different: promiscuity and diversity in the molecular mechanisms of action of the aryl hydrocarbon (dioxin) receptor, Toxicol. Sci. 124: 1–22. https://doi.org/10.1093/toxsci/kfr218 PMID: 21908767
9. Shinkyo R, Sakaki T, Ohta M, Inouye K. 2003 Metabolic pathways of dioxin by CYP1A1: species difference between rat and human CYP1A subfamily in the metabolism of dioxins, Arch. Biochem. Biophys. 409: 180–187. https://doi.org/10.1016/s0003-9861(02)00366-1 PMID: 12464257
10. Van den Berg M, Birnbaum LS, Denison M, De Vito M, Farland W, Feeley M, et al. 2006 The 2005 World Health Organization reevaluation of human and mammalian toxic equivalency factors for dioxins and dioxin-like compounds. Toxicol. Sci. 93: 223–241. https://doi.org/10.1093/toxsci/kfl055 PMID: 16829543
11. Inouye K, Shinkyo R, Takita T, Ohta M, Sakaki T. 2002 Metabolism of polychlorinated dibenzo-p-dioxins (PCDDs) by human cytochrome P450-dependent monooxygenase systems, J. Agric. Food Chem. 50: 5496–5502. https://doi.org/10.1021/jf020415z PMID: 12207498
12. Molcan T, Swigonska S, Nynca A, Sadowska A, Ruszkowska M, Orlowska K, et al. 2019 Is CYP1B1 involved in the metabolizm of dioxins in the pig? BBA General Subjects, 1863: 291–303. https://doi.org/10.1016/j.bbagen.2018.09.024 PMID: 30278240
13. Larsen JC. 2006 Risk assessments of polychlorinated dibenzo- p-dioxins, polychlorinated dibenzofurans, and dioxin-like polychlorinated biphenyls in food, Mol. Nutr. Food. Res. 50: 885–896. https://doi.org/10.1002/mnfr.200500247 PMID: 17009211
14. Sorg O, Zennegg M, Schmid P, Fedosyuk R, Valikhnovskyi R, Gaide O, et al. 2009 2,3,7,8-tetrachlorodibenzo-p-dioxin (TCDD) poisoning in Victor Yushchenko: identification and measurement of TCDD metabolites, Lancet. 374: 1179–1185. https://doi.org/10.1016/S0140-6736(09)60912-0 PMID: 19660807
15. Mimura J, Fujii-Kuriyama Y. 2003 Functional role of AhR in the expression of toxic effects by TCDD. BBA General Subjects 1619: 263–268. https://doi.org/10.1016/s0304-4165(02)00485-3 PMID: 12573486
16. Go R-E, Hwang K-A, Choi K-C. 2015 Cytochrome P450 1 family and cancers. J. Ster. Bioch. Mol. Biol. 147:24–30. https://doi.org/10.1016/j.jsbmb.2014.11.003 PMID: 25448748

17. Messina A, Siniscalco A, Puccinelli E, Gervasi PG, Longo V. 2012 Cloning and tissues expressions of the pig CYP1B1 and CYP2J34. Res. Vet. Sci. 92: 438–443. https://doi.org/10.1016/j.rvsc.2011.04.012 PMID: 21550618

18. Tsang H, Cheung TY, Kodithuwakku SP, Chai J, Jeung WS, Wong CK, et al. 2012 2,3,7,8-Tetrachlorodibenzo-p-dioxin (TCDD) suppresses spheroids attachment on endometrial epithelial cells through the down-regulation of the Wnt-signaling pathway. Reprod. Toxicol. 33:60–66. https://doi.org/10.1016/j.reprotox.2011.11.002 PMID: 22134133

19. Molcan T, Swigonska S, Orlowska K, Myszczynski K, Nynca A, Sadowska A, et al. 2017 Structural-functional adaptations of porcine CYP1A1 to metabolize polychlorinated dibenzo-p-dioxins, Chemosphere. 168: 205–216. https://doi.org/10.1016/j.chemosphere.2016.10.035 PMID: 27783961

20. Cojocaru V, Winn PJ, Wade RC. 2007 The ins and outs of cytochrome P450s. Bioch. Bioph. Acta, 1770: 390–401. https://doi.org/10.1016/j.bbagen.2006.07.005 PMID: 16920266

21. Kwon Y-J, Shin S, Chun Y-J. 2021 Biological roles of cytochromes P450 1A1, 1A2 and 1B1 enzymes. Arch. Pharm. Res. 44: 63–83. https://doi.org/10.1007/s12272-021-01306-w PMID: 33484438

22. McKinnon RA, McManus ME. 1996 Localization of cytochromes P450 in human tissues: implications for chemical toxicity. Pathology 28: 148–155. https://doi.org/10.1080/00313029600169783 PMID: 8743822

23. Schelstraete W, De Clerck L, Govaert E, Millecam J, Devreese M, Deforce D, et al. 2019 Characterization of Porcine Hepatic and Intestinal Drug Metabolizing CYP450: Comparison with Human Orthologues from A Quantitative, Activity and Selectivity Perspective. Sci.Rep. 9:9233. https://doi.org/10.1038/s41598-019-45212-0 PMID: 31239454

24. Hakk H, Diliberto JJ, Birnbaum LS. 2009 The effect of dose on 2,3,7,8-TCDD tissue distribution, metabolism and elimination in CYP1A2 (-/-) knockout and C57BL/6N parental strains of mice. Toxicol. Appl. Pharmacol., 241: 119–126. https://doi.org/10.1016/j.taap.2009.08.009 PMID: 19695277

25. Inui H, Itoh T, Yamamoto K, Ikushiro S, Sakaki T. 2014 Mammalian cytochrome P450-dependent metabolism of polychlorinated dibenzo-p-dioxins and coplanar polychlorinated biphenyls, Int. J. Mol. Sci., 15: 14044–14057. https://doi.org/10.3390/ijms150814044 PMID: 25123135

26. Wang C, Tang Z, Zhang Y, Liang Y, Song F, Cai Z. 2013 A new method for identification of an in vitro metabolites of 2,3,7,8-TCDD with rat liver microsomes by using liquid chromatography-mass spectrometry. Anal. Methods 11: 2757–2761.

27. Poiger H, Buser HR, Weber H, Zweifel U, Schlatter C. 1982 Structure elucidation of mammalian TCDD–metabolites. In: Tucker R.E., Young A.L., Gray A.P. (eds) Human and environmental risks of chlorinated dioxins and related compounds. Environmental Science Research, Springer, Boston, 38: 484–486.

28. Matter H, Nazaré M, Güssregen S, Will DW, Schreuder H, Bauer A, et al. 2009 Evidence for C-Cl/C-Br. . .Pi interactions as an important contribution to protein-ligand binding affinity, Angew. Chem. Int. Ed. Engl. 48: 2911–2916. https://doi.org/10.1002/anie.200806219 PMID: 19294721

29. Wilcken R, Zimmermann MO, Lange A, Joerger AC, Boeckler FM. 2013 Principles and applications of halogen bonding in medicinal chemistry and chemical biology. J. Med. Chem. 56: 1363–1388. https://doi.org/10.1021/jm3012068 PMID: 23145854

30. Xu Z, Yang Z, Liu Y, Lu Y, Chen K, Zhu W. 2014 Halogen bond: its role beyond drug-target binding affinity for drug discovery and development. J. Chem. Inf. Model. 54: 69–78. https://doi.org/10.1021/ci400539q PMID: 24372485

31. Dubey KD, Wang B, Shaik S. 2016 Molecular dynamics and QM/MM calculations predict the substrate-induced gating of cytochrome P450 BM3 and the regio- and stereo selectivity of fatty acid hydroxylation, J. Am. Chem. Soc. 138: 837–845. https://doi.org/10.1021/jacs.5b08737 PMID: 26716578

32. Lonsdale R, Fort RM, Rydberg P, Harvey JN, Mulholland AJ. 2016 Quantum mechanics/molecular mechanics modeling of drug metabolism: mexiletine N-hydroxylation by cytochrome P450 1A2. Chem. Res. Toxicol. 29: 963–971. https://doi.org/10.1021/acs.chemrestox.5b00514 PMID: 27064685

33. Urban P, Truan G, Pompon D. 2015 Access channels to the buried active site control substrate specificity in CYP1A P450 enzymes. Biochim. Biophys. Acta, 1850: 696–707. https://doi.org/10.1016/j.bbagen.2014.12.015 PMID: 25529298

34. Uehara S, Uno Y, Inoue T, Sasaki E, Yamazaki H. 2016 Molecular cloning, tissue distribution and functional characterization of marmoset cytochrome P450 1A1, 1A2 and 1B1. Drug Metab. Dispos. 44: 8–15. https://doi.org/10.1124/dmd.115.067561 PMID: 26502772

35. Edgar RC. 2004 MUSCLE: multiple sequence alignment with high accuracy and high throughput, Nucleic. Acids. Res. 32:1792–1797. https://doi.org/10.1093/nar/gkh340 PMID: 15034147

36. Eswar N, Marti-Renom MA, Webb B, Madhusudhan MS, Eramian D, Shen M, et al. 2006 Comparative protein structure modeling with MODELLER, Curr. Prot. Bioinf. S15: 1–30. https://doi.org/10.1002/0471250953.bi0506s15 PMID: 18428767

37. Bowie JU, Lüthy R, Eisenberg D 1991 A method to identify protein sequences that fold into a known three-dimensional structure, Science. 253 164–170. https://doi.org/10.1126/science.1853201 PMID: 1853201

38. Laskowski RA, MacArthur MW, Moss DS, Thornton JM 1993 PROCHECK—a program to check the stereochemical quality of protein structures, J. Appl. Cryst. 26: 283–291.

39. Sippl MJ. 1993 Recognition of errors in three-dimensional structures of proteins, Proteins 17: 355–362. https://doi.org/10.1002/prot.340170404 PMID: 8108378

40. Wiederstein M, Sippl M. 2007 ProSA-web: interactive web service for the recognition of errors in three-dimensional structures of proteins. Nucleic. Acids. Res. 35:407–410 https://doi.org/10.1093/nar/gkm290 PMID: 17517781

41. Kleywegt GJ, Jones TA. 1994 Detection, delineation, measurement and display of cavities in macromolecular structures, Biol. Crystallogr. 50:178–185. https://doi.org/10.1107/S0907444993011333 PMID: 15299456

42. Irwin T, Sterling MM, Mysinger ES, Bolstad R, Coleman G. 2012 ZINC: a free tool to discover chemistry for biology, J. Chem. Inf. Model. 52:1757–1768. https://doi.org/10.1021/ci3001277 PMID: 22587354

43. Morris GM, Huey R, Lindstrom W, Sanner MF, Belew RK, Goodsell DS, et al. 2009 Autodock4 and AutoDockTools4: automated docking with selective receptor flexibility. J. Comput. Chem. 30:2785–2791. https://doi.org/10.1002/jcc.21256 PMID: 19399780

44. Shahrokh K, Orendt A, Yost GS, Cheatham TE. 2012 Quantum mechanically derived AMBER-compatible heme parameters for various states of the cytochrome P450 catalytic cycle, J. Comput. Chem. 33:119–133. https://doi.org/10.1002/jcc.21922 PMID: 21997754

45. Trott O, Olson AJ. 2010 AutoDock Vina: improving the speed and accuracy of docking with a new scoring function, efficient optimization and multithreading, J. Comput. Chem. 31: 455–461. https://doi.org/10.1002/jcc.21334 PMID: 19499576

46. Abrahama MJ, Murtolad T, Schulz R, Pálla S, Smith JC, Hessa B, et al. 2015 GROMACS: high performance molecular simulations through multi-level parallelism from laptops to supercomputers, Software X. 1–2: 19–25.

47. Hornak V, Abel R, Okur A, Strockbine B, Roitberg A, Simmerling C. 2006 Comparison of multiple Amber force fields and development of improved protein backbone parameters, Proteins. 65: 712–25. https://doi.org/10.1002/prot.21123 PMID: 16981200

48. Frisch MJ, Trucks GW, Schlegel HB, Scuseria GE, Robb MA, Cheeseman JR, et. al. 2009 Gaussian 09 (Gaussian, Inc., Wallingford CT, 2009).

49. Cieplak P, Cornell WD, Bayly C, Kollman PA. 1995 Application of the multimolecule and multiconformational RESP methodology to biopolymers: charge derivation for DNA, RNA and proteins, J. Comput. Chem. 16:1357–1377.

50. Price DJ, Brooks CL. 2004 A modified TIP3P water potential for simulation with ewald summation, J. Chem. Phys. 121:10096–10103. https://doi.org/10.1063/1.1808117 PMID: 15549884

51. Hess B, Bekker H, Berendsen JC, Fraaije JGEM. 1997 LINCS: a linear constraint solver for molecular simulations, J. Comp. Chem. 18:1463–1472.

52. Boresh S, Tettinger F, Leitgeb M. 2003 Absolute Binding Free Energies: A Quantitative approach for their calculation, J. Phys. Chem. B, 107, 9535–9551.

53. Kirkwood JG. 1935 Statistical Mechanics of Fluid Mixtures, J. Chem. Phys. 3, 300.

54. Chovancova E, Pavelka A, Benes P, Strnad O, Brezovsky J, Kozlikova B, et al. 2012 CAVER 3.0: a tool for the analysis of transport pathways in dynamic protein structures, PLoS Comput. Biol. 10:1–10. https://doi.org/10.1371/journal.pcbi.1002708 PMID: 23093919

55. DeLano WL. 2002 The PyMOL Molecular Graphics System; Version 1.7, Schroinger LLC.